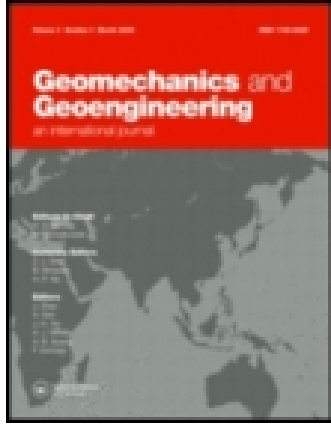


This article was downloaded by: [Dalian University of Technology]

On: 10 April 2015, At: 05:48

Publisher: Taylor & Francis

Informa Ltd Registered in England and Wales Registered Number: 1072954 Registered office: Mortimer House, 37-41 Mortimer Street, London W1T 3JH, UK



Geomechanics and Geoengineering: An International Journal

Publication details, including instructions for authors and subscription information:

<http://www.tandfonline.com/loi/tgeo20>

Discrete element analysis of breakage of irregularly shaped railway ballast

Ying Yan^a, Jinfeng Zhao^b & Shunying Ji^b

^a School of Civil and Safety Engineering, Dalian Jiaotong University, Dalian, China

^b State Key Laboratory of Structural Analysis for Industrial Equipment, Dalian University of Technology, Dalian, China

Published online: 15 Jul 2014.



[Click for updates](#)

To cite this article: Ying Yan, Jinfeng Zhao & Shunying Ji (2015) Discrete element analysis of breakage of irregularly shaped railway ballast, Geomechanics and Geoengineering: An International Journal, 10:1, 1-9, DOI: [10.1080/17486025.2014.933891](https://doi.org/10.1080/17486025.2014.933891)

To link to this article: <http://dx.doi.org/10.1080/17486025.2014.933891>

PLEASE SCROLL DOWN FOR ARTICLE

Taylor & Francis makes every effort to ensure the accuracy of all the information (the "Content") contained in the publications on our platform. However, Taylor & Francis, our agents, and our licensors make no representations or warranties whatsoever as to the accuracy, completeness, or suitability for any purpose of the Content. Any opinions and views expressed in this publication are the opinions and views of the authors, and are not the views of or endorsed by Taylor & Francis. The accuracy of the Content should not be relied upon and should be independently verified with primary sources of information. Taylor and Francis shall not be liable for any losses, actions, claims, proceedings, demands, costs, expenses, damages, and other liabilities whatsoever or howsoever caused arising directly or indirectly in connection with, in relation to or arising out of the use of the Content.

This article may be used for research, teaching, and private study purposes. Any substantial or systematic reproduction, redistribution, reselling, loan, sub-licensing, systematic supply, or distribution in any form to anyone is expressly forbidden. Terms & Conditions of access and use can be found at <http://www.tandfonline.com/page/terms-and-conditions>

Discrete element analysis of breakage of irregularly shaped railway ballast

Ying Yan^a, Jinfeng Zhao^b and Shunying Ji^{b*}

^aSchool of Civil and Safety Engineering, Dalian Jiaotong University, Dalian, China; ^bState Key Laboratory of Structural Analysis for Industrial Equipment, Dalian University of Technology, Dalian, China

(Received 9 August 2013; accepted 5 June 2014)

In order to reduce the maintenance costs of ballasted railway track and improve passenger comfort, the railway ballast particle breakage and its effect on track settlement need to be better understood. The failure process of individual railway ballast loaded between flat platens is simulated using the discrete element method, considering its irregular shape with the incorporation of parallel bonds. The tensile strength, the stress of a survival probability of 37% of samples, is obtained and compared with laboratory results from published literature for the verification of DEM simulations. The evolution to failure of the particle is understood from the stress-strain curve and progressive failure modes. The internal breakage mechanisms are analysed by tracking the accumulation of bond breakage number and the contact force distributions.

Keywords: discrete element method; breakage; irregular shape; parallel bond; railway ballast

Introduction

Traditional ballasted railway track is applied worldwide. The main benefits of this type of track are the relatively low construction costs, high elasticity, high noise absorption and high maintainability at relatively low cost (Esveld 1989). However, ballast is one of the main sources of track deterioration due to its discrete nature (Selig and Waters 1994). The deterioration is evidenced by the rearrangement and breakage of ballast particles. Ballast breakage directly contributes to ballast degradation on one hand, and may produce differential settlement of the track due to the stress redistribution on the other hand. Past studies have reported that ballast breakage has a substantial effect on track settlement. Track deformation strongly increases even though only a few particles break (Lobo-Guerrero and Vallejo 2006, Housain *et al.* 2007). In particular, as a consequence of ever-increasing train speeds and axle loads, ballast breakage and track settlement have become more and more important. Thereby, a better fundamental understanding of the ballast breakage mechanism and its effect on track settlement plays a major role in reducing the maintenance costs of ballasted track and improving passenger comfort as well. In this study, we investigate the breakage of railway ballast via a numerical study.

The breakage mechanism of ballast is complex. It can basically be classified as breakage of asperities and particle splitting (Indraratna *et al.* 2009). Individual particle breakage tests can offer an insight into the fracture mechanism and tensile strength of railway ballast. It is widely accepted that the

crushing of an individual particle is in fact a tensile failure when loaded between platens, although the tensile failure under diametric loading was put in doubt by different authors (Darvell 1990, Russell and Muir Wood 2009). The tensile strength can be indirectly measured by compressing the particle between two parallel platens up to failure with the splitting of the particle into two or more smaller pieces (Jaeger 1967, McDowell and Bolton 1998, Lim *et al.* 2004). Lim *et al.* (2004) quantified that the tensile strengths of railway ballast follow the Weibull distribution well for a given size based on laboratory data. The probability of breakage also increases with an increase in ballast size.

The discrete element method (DEM), with the advantages of providing a microscopic insight of the progressive failure phenomena and breakage mechanism, has shown to be a useful tool in the numerical simulations of crushable granular solids. Basically, there are two ways of describing individual particle breakage using the DEM. The individual particle is either modelled by an agglomerate of bonded spheres (Kun and Herrmann 1996, Cheng *et al.* 2003, 2004, Potyondy and Cundall 2004, Lim and McDowell 2005, Indraratna *et al.* 2010, Cil and Alshibli 2012) or replaced by a group of fragments based on suitable failure criteria (Lobo-Guerrero and Vallejo 2006, Housain *et al.* 2007).

Ballast particles are of irregular shape naturally. Clumps formed by clumping or agglomerates formed by bonding multiple spheres, offer an effective way to model realistic particles because of the simple contact detection and force calculation between spheres. Clumped particles are created by clumping

*Corresponding author. Email: jisy@dlut.edu.cn

spheres with prescribed initial overlap without generating interaction force, and all of clumped particles move as one element that will not break apart (Itasca 1999, Peters and Dziugys 2002, Ferellec and McDowell 2008, 2010). Aggregates of bonded spheres, created by bonding regular particles without initial overlap, are allowed to break up under large particle interaction and deformation (Itasca 1999, Potyondy and Cundall 2004, Indraratna *et al.* 2010). Therefore, bonding models are more suitable for the simulation of irregularly shaped ballast particle breakage, since they are capable of describing arbitrary shapes and allowing breakage at the same time.

However, previous bonding models employed a two-dimensional disc or three-dimensional spherical agglomerate to resemble the particle, neglecting the realistic irregular shape when modelling breakage (Cheng *et al.* 2003, 2004, Lim and McDowell 2005, Cil and Alshibli 2012). It was noted that particle shape not only governs breakage strength, but also influences the macro behaviours of railway ballast (Tang *et al.* 2001, Lim and McDowell 2005, Cho *et al.* 2006). With the finite element method, Tang *et al.* (2001) simulated a 2-D single particle breakage, and reported that the more spherical the particles are, the higher the breakage strength is. Hence, it is necessary to take into account the particle shape in the DEM modelling of ballast breakage.

In the sphere bonding models, there are two specific implementations, namely, parallel bond and contact bond (Itasca 1999, Potyondy and Cundall 2004). In the parallel bond, a bond disk is defined between the two bonded spheres to transfer normal force, shear force and bending moment or oppose rolling. The contact bond model does not have the bond disk as defined in the parallel bond model, and can only resist normal and shear forces at the contact point. The contact bond model has been adopted in the simulation of ballast as an agglomerate of bonded spheres (Cheng *et al.* 2003, 2004, Lim and McDowell 2005). Similar to the contact bond model but with only the normal force resisted, Ergenzinger *et al.* (2012) simulated the breakage of angular ballast and the oedometric compression tests using the software package Pasimodo. In addition, Indraratna *et al.* (2010) constructed irregular ballast particles with the parallel bond model by modelling their 2D projections and simulated the permanent deformation and degradation of ballast under cyclic loading with different frequencies. The mechanical behaviours of ballast simulated were compared well with the experimental data. In this study, the parallel model is adopted.

The objective of this study is to generate a more realistic DEM model of ballast breakage, considering its irregular shape with the incorporation of parallel bonds. The simulations are performed using SDEM code (sphere-based discrete element method), which was developed by the authors. This code has been applied to simulate the mechanical behaviours of granular rock with the ability to model irregular-shaped particles by using overlapped spheres, bonded spheres and dilated polyhedron, respectively (Yan and Ji, 2010; Ji, 2013; Ji and Di, 2013). In this study, the simulated results with SDEM are

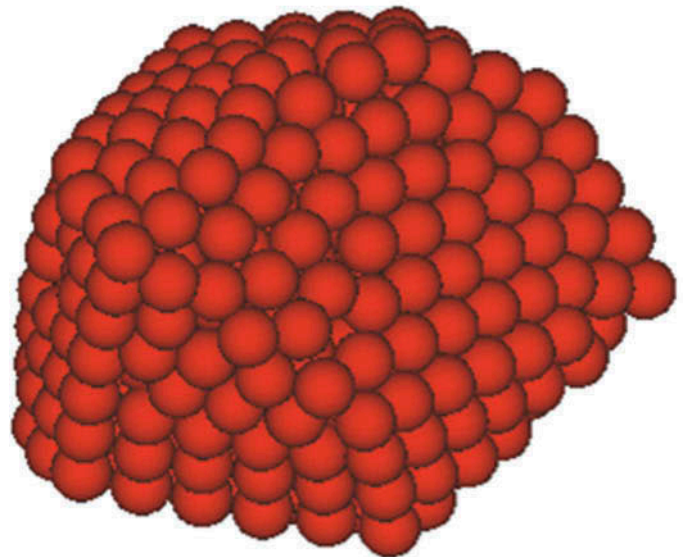
validated by available data from published literature. The breakage mechanism is further analysed through bond breakage and contact force distributions at microscopic scale.

DEM model of ballast particles with parallel bonds

Figure 1a is the picture of a real ballast particle. A more realistic shape description is a prerequisite for a more accurate simulation of its mechanical behaviours. To this end, individual ballast particles are constructed as an agglomerate of a large number of small spheres that are connected by parallel bonds.



(a)



(b)

Figure 1. Realistic ballast particle and its DEM model: (a) Realistic ballast particle; (b) DEM model.

Parallel bond model

In this study, uniform spheres are bonded together to generate irregularly shaped ballast particles with various packing patterns. The corresponding parallel bond is shown in Figure 2a. Here, \mathbf{x}_A and \mathbf{x}_B are the position vector of sphere A and sphere B , \mathbf{n} is the contact normal vector. However, non-uniform spheres can also be adopted to improve the geometric accuracy of ballast particles. This method has been applied in the construction of irregular rock rubbles with overlapped spheres (Ferrellec and McDowell 2008, 2010). As a result of the constant normal and shear stiffness of the bond, a force and a moment are developed within the bond induced by the relative motion at the contact. The force and moment can be resolved into normal and shear components, \mathbf{F}_n and \mathbf{F}_s , \mathbf{M}_n and \mathbf{M}_s . The

maximum normal and shear stresses acting at the bond periphery can be written as

$$\sigma_{\max} = \frac{|\mathbf{F}_n|}{A} + \frac{|\mathbf{M}_s|}{I} \tag{1}$$

$$\tau_{\max} = \frac{|\mathbf{F}_s|}{A} + \frac{|\mathbf{M}_n|}{J} \tag{2}$$

where R is the bonding radius and set as the sphere radius. $A = \pi R^2$, $I = \pi R^4/4$ and $J = \pi R^4/2$ are the area, inertia moment and polar inertia moment of the bonding disk, respectively.

If either the maximum normal stress or the maximum shear stress exceeds the corresponding normal strength and shear strength, the parallel bond breaks and is deleted. The deletion of bonds describes the crack initiation and propagation. In this way, the failure phenomena and final splitting can be directly reproduced. In this study, the normal strengths are randomly generated as a normal probability distribution with the mean of 25.0 MPa and standard deviation of 2.0 MPa. For the bonded discrete element method for rock materials, a ratio of the shear strength to the normal strength can be defined. In the study of Potyondy and Cundall (2004), the shear strength equals the normal strength. This relationship is also applied to the simulation of bonded rocks and agglomerates (Cho *et al.* 2007, Hanley *et al.* 2011). Here, the shear strengths are also set as the same as those normal ones.

For the contact point interaction between sub-spheres, the linear visco-elastic model with the Mohr-Coulomb friction law is adopted, as shown in Figure 2b. Here M_A and M_B are the mass of sphere A and B , K_n and K_s are the normal and tangential stiffness, C_n and C_s are the normal and tangential damping coefficient, μ is the friction coefficient.

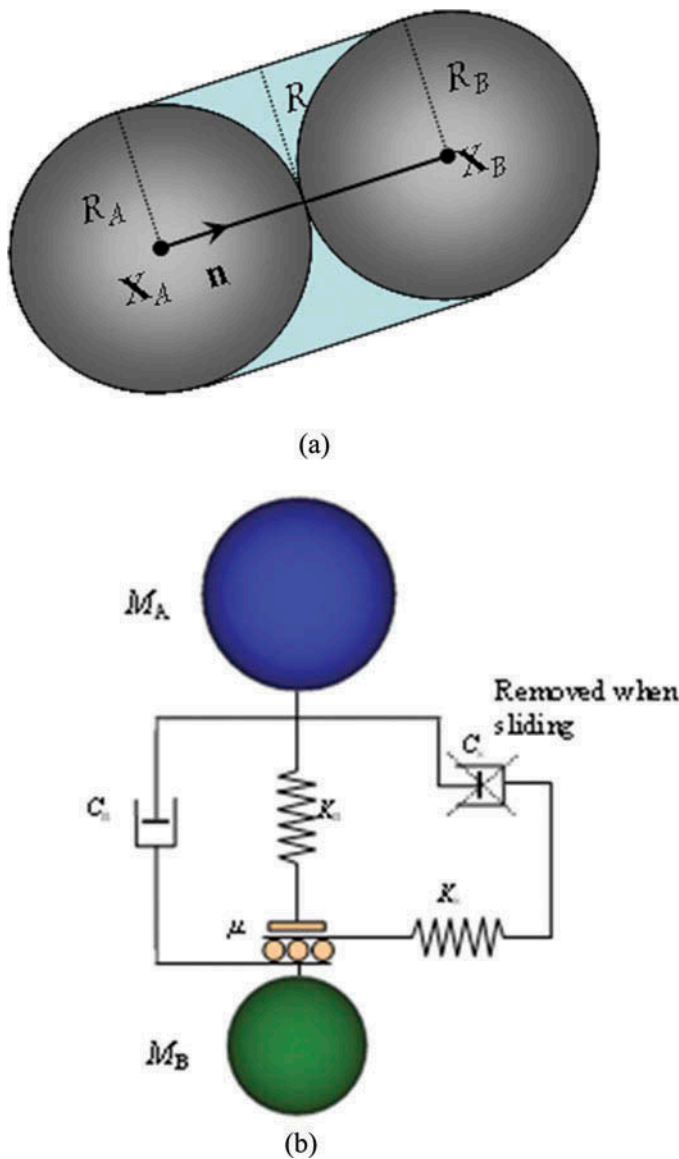


Figure 2. Interaction between sub-spheres: (a) Parallel bond model; (b) Contact force model.

Generation of irregularly shaped ballast particle

Since railway ballast features many planar surfaces, convex polyhedron are used to resemble the realistic ballast particle shapes. Figure 3 shows the generation of a single ballast particle. An arbitrary convex polyhedron is first generated and its surfaces are extracted as the ballast particle surfaces (Figure 3a). The size and shape of ballast are both considered during the polyhedron generation. In this study, the mean sizes of ballast particles are in the range of [37 mm, 51 mm]. The ratio of the ballast length to width is in the range of [1.5, 3.0], which is defined with the measurement of ballast particles. A cubic domain just encompassing the space enclosed by these surfaces is defined next, with a uniformly sized assembly of spheres filled into it with a hexagonal close packing (HCP) (Figure 3b). The system is then stabilised by a cycling process under gravity until reaching equilibrium (Figure 3c). Those spheres located inside the space enclosed by the ballast particle surfaces remain to form the final ballast particle. Finally, parallel bonds are installed at existing contacts and between those

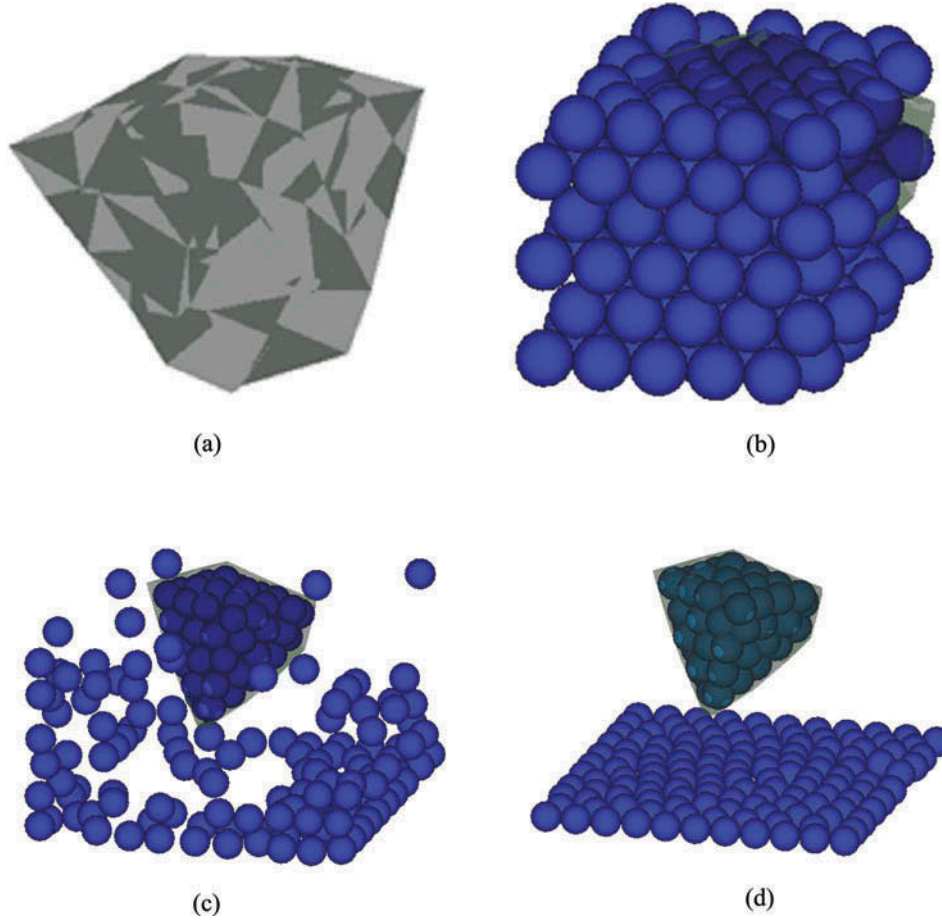


Figure 3. The generation of a single ballast particle DEM model: (a) The generated surfaces; (b) Spheres packed in the cubic domain; (c) Stabilization process; (d) The final model.

spheres that are within a certain distance of one another (Figure 3d). Figure 1b gives the corresponding DEM model of the ballast particle shown in Figure 1a. This ballast particle is generated by 331 sub-spheres with 1073 initial bonds.

Behaviour of individual ballast particle breakage

Individual ballast particle breakage tests conducted by Lim *et al.* (2004) are used for validation of the developed DEM model. Here, 33 ballast particles are constructed randomly within the range of [37 mm, 51 mm]. Ballast particles can be modelled more realistically with smaller sub-spheres, however, the computational cost increases dramatically in the DEM simulations. Here, the diameter of sub-spheres is selected as 5 mm. The corresponding sub-sphere number is in the range of [258~575]. The computational parameters values are selected based on some related references (Lobo-Guerrero and Vallejo 2006, Housain *et al.* 2007, Lim and McDowell 2007, Ji and Di 2013). The normal stiffness is related to the particle elastic modulus E , the particle diameter D as $K_n = \pi DE/4$ (Ji *et al.* 2009). The ratio of normal stiffness to shear stiffness is set as

2.0. The elastic modulus of ballast $E = 70$ GPa, the inter-particle friction coefficient $\mu_{p-p} = 0.5$, the inter-particle restitution coefficient $e_{p-p} = 0.5$, and the ballast density $\rho = 2650$ kg/m³.

Tensile strength of railway ballast with Weibull statistics

The ballast tensile strengths have been reported to follow Weibull statistics well (Lim *et al.* 2004). The survival probability P_s under a tensile stress σ is given by (McDowell and Amon 2000),

$$P_s = \exp\left[-\left(\frac{\sigma}{\sigma_0}\right)^m\right] \quad (3)$$

where σ_0 is the stress to give a survival probability of 37%, m is the Weibull modulus.

By rewriting Equation (3), a linear relationship can be obtained between $\ln[\ln(1/P_s)]$ and $\ln \sigma$ as,

$$\ln\left[\ln\left(\frac{1}{P_s}\right)\right] = m \ln \sigma - m \ln \sigma_0 \quad (4)$$

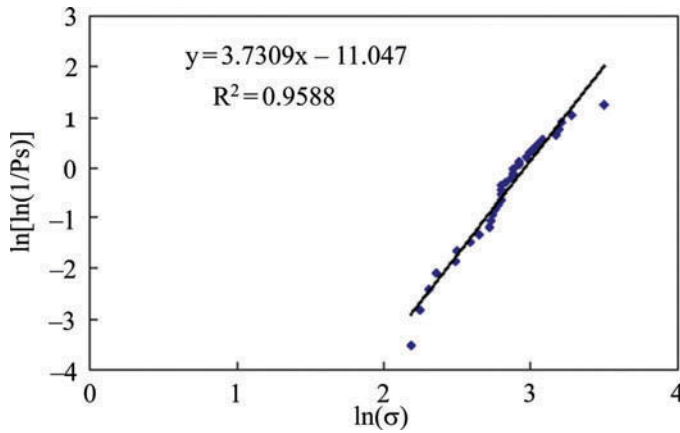


Figure 4. Weibull survival probability plot.

Taking $\ln \sigma$ as the x coordinate and $\ln(\ln(1/P_s))$ as the y coordinate, the Weibull modulus m and the 37% tensile stress σ_0 are the slope and y -intercept of the linear fit of the set of data for a given size of ballast, respectively. Here, the induced tensile stress σ for an individual particle of average size d loaded under a force F is defined as (McDowell and Amon 2000, Ergenzinger *et al.* 2012),

$$\sigma = \frac{F}{d^2} \quad (5)$$

The survival probability P_s can be calculated using the mean rank position (Davidge 1979),

$$P_s = 1 - \frac{i}{N + 1} \quad (6)$$

where i is the i th ranked sample from a total of N .

Figure 4 depicts the simulation results fitted with a Weibull survival probability curve. The 37% tensile stress and the Weibull modulus m are calculated as $\sigma_0 = 19.3$ MPa and $m = 3.73$. The simulated results agree well with the laboratory results of $\sigma_0 = 21.7$ MPa and $m = 3.07$ from Lim *et al.* (2004).

It is also noted that, the tensile strength $\sigma_0 = 19.3$ MPa obtained with the developed model is less than that simulated by Lim and McDowell (2005) as $\sigma_0 = 22.4$ MPa. The reason is that their ballast particle models were close to spherical in shape. This supports the conclusion that the more spherical the particles are, the higher the breakage strength is (Hess and Schonert 1981).

Stress-strain analysis

The stress-strain relationship can be used to understand different phases of the failure development. Figure 5 plots the stress-strain curve of a typical ballast particle of size 41.68 mm during compression. The stress-strain curve can be divided into four stages: linear elastic ($O-A$), crack initiation ($A-C$), softening ($C-D$) and final splitting ($E-G$). In the linear elastic

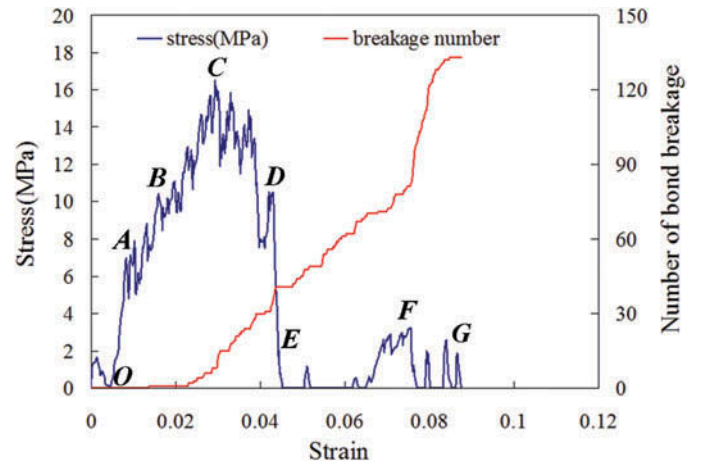


Figure 5. Stress-strain curve and number of bond breakage of a typical ballast particle.

stage, the stress-strain curve is almost a line, the particle deforms linearly. Then the crack initiates, and deformation happens and a series of local sub-peaks exist prior to the stress peak at point C. This is because of the fracture of asperities of the ballast particle at their contacts with the platen. The elastic energy will be transformed to kinetic energy during the breakage of bonded disks (Ji and Di 2013). Meanwhile, the bearing capacity of damaged ballast drops a little when two bonded spheres break. It can also induce the stress fluctuation in the ballast fracture process. The stress peak of 16.47 MPa appears at the strain $\epsilon = 0.029$. After that the particle enters the softening stage, with a drop in stress and more cracks formed. These cracks gradually connect to each other, until the ballast particle is seen to split into two smaller pieces.

Figure 6 depicts the progressive failure modes correspondingly. Here, the sub-spheres colouring scheme is based on the fragment size. The sub-sphere colour changes during the breakage process due to the fragment size change. The initial green represents the ballast particle is intact as one large piece, while the sub-spheres with smaller fragments are coloured in blue. As shown in Figure 6a, there is no bond breakage in the linear elastic stage. Figure 6b shows few bond breaks as an indication of crack initiation. Cracks start from the contacts between the particle and the upper platen, parallel to the direction of loading. Breakage aggravates during the softening stage as shown in Figure 6d. The particle starts to break until its final splitting along the loading direction as shown in Figure 6e and Figure 6f, respectively.

Micro analysis of the breakage mechanisms

Bond breakage number

The macro change from local damage to final splitting of the ballast particle is attributed to the accumulation of bond breakage at the microscopic scale. Figure 5 also plots the

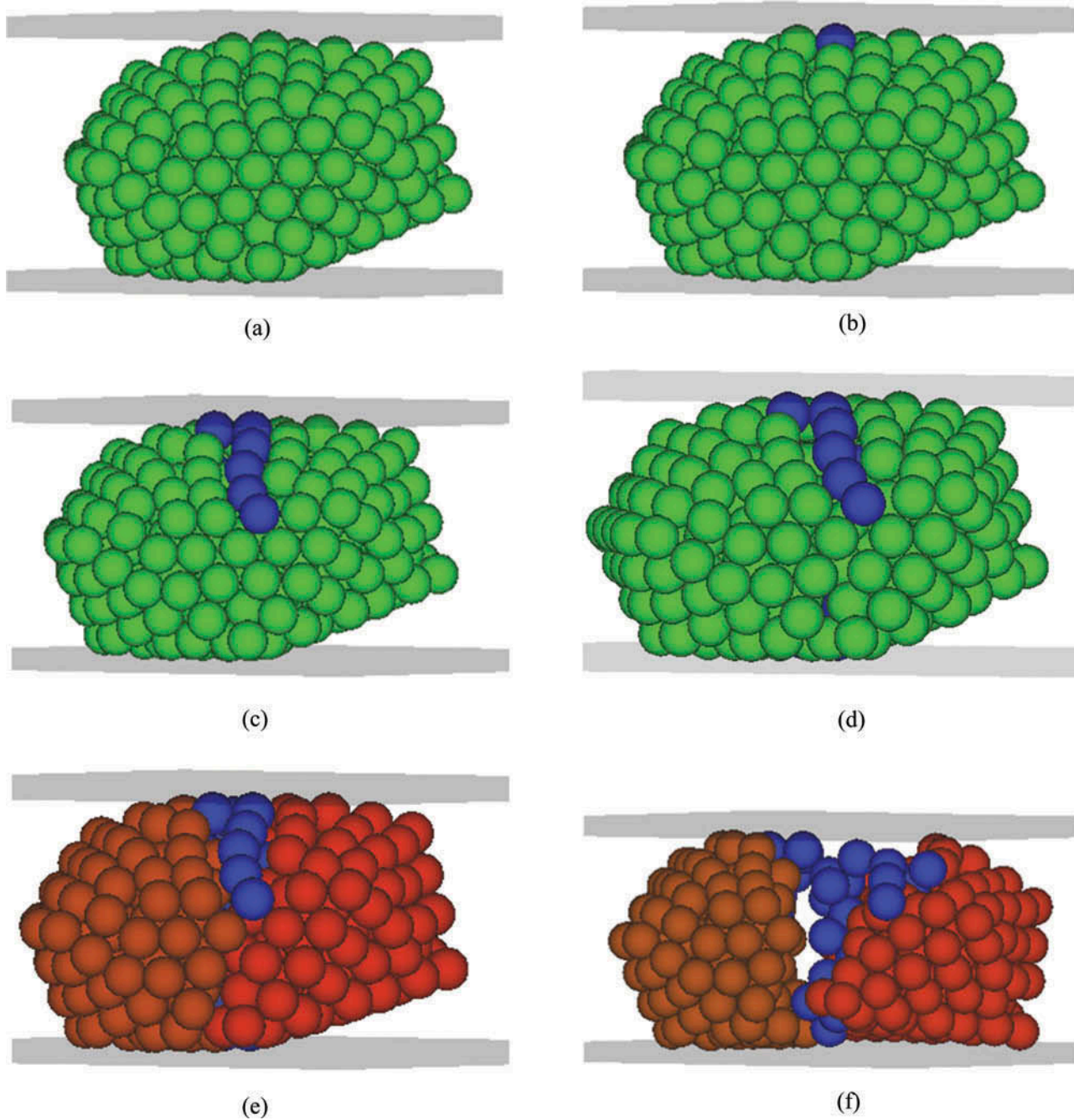


Figure 6. Progressive failure modes of a single ballast particle during compression: (a) $\varepsilon = 0.0092$; (b) $\varepsilon = 0.015$; (c) $\varepsilon = 0.029$; (d) $\varepsilon = 0.043$; (e) $\varepsilon = 0.045$; (f) $\varepsilon = 0.076$.

accumulative number of bond breakages during the whole failure process. It shows that no bonds break in the elastic stage. Then the number of bond breakages increases steadily in the crack initiation stage. The first bond breaks at the strain $\varepsilon = 0.014$. In the softening stage, each decrease of the stress accompanies a big increase in the number of bond breakages. The number of bond breakages continues to increase rapidly as the particle enters the final splitting stage. During the whole failure process of the ballast particle, there are a total of 133 bond breakages, including 130 tensile breakages and three

shear ones. This is an indication that tensile failure dominates when an individual particle is loaded between platens, which accounts for 98% of the total breakages.

Contact force distributions

The degree of breakage can also be explained by the structure of the contact force distributions. Figure 7 depicts the distributions of the corresponding normal contact forces. The lines of contact

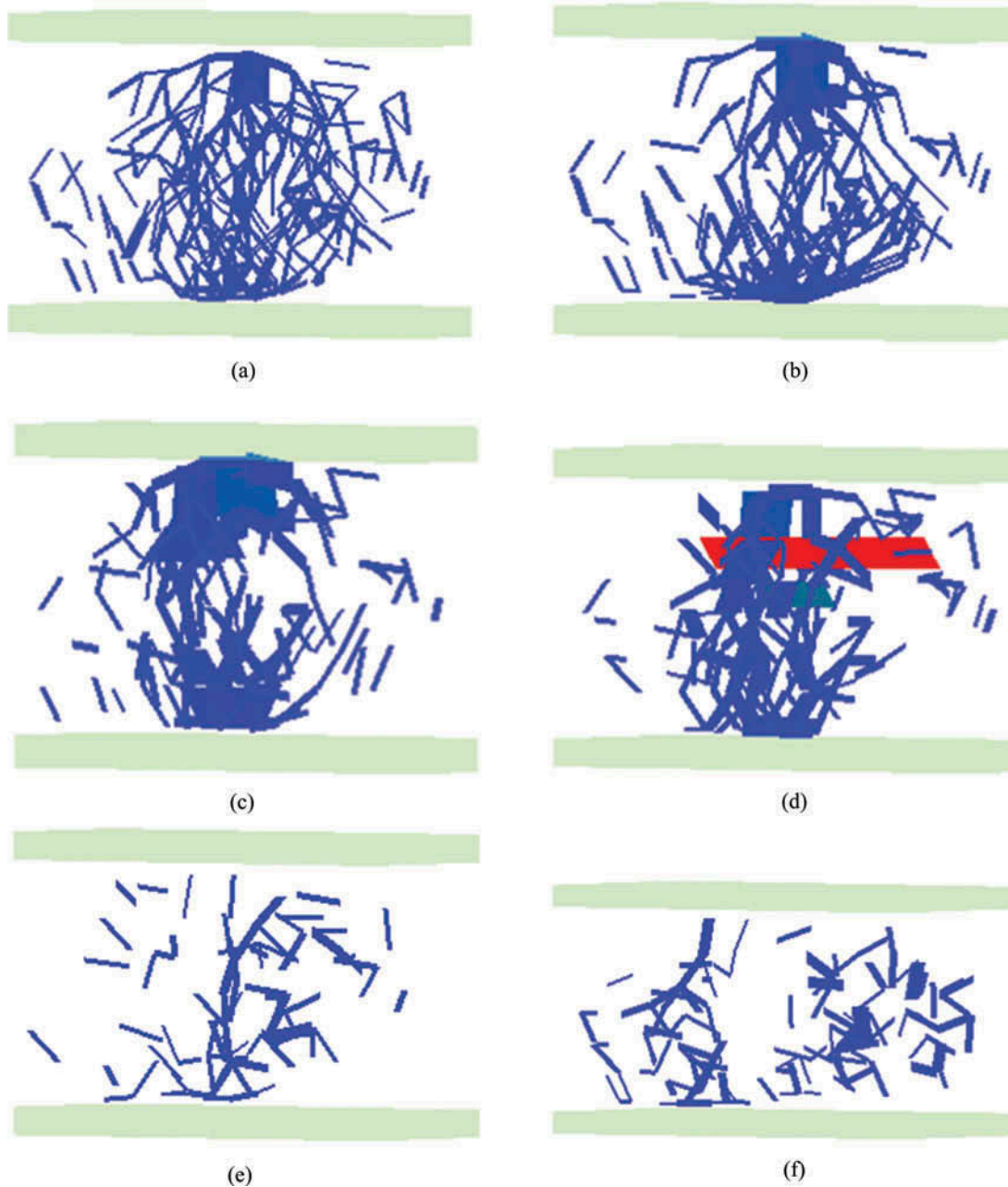


Figure 7. Contact force distributions at different strains: (a) $\epsilon = 0.0092$; (b) $\epsilon = 0.015$; (c) $\epsilon = 0.029$; (d) $\epsilon = 0.043$; (e) $\epsilon = 0.045$; (f) $\epsilon = 0.076$.

forces are linked between the centres of spheres in contact. In these figures, the thicknesses and different colours of the lines represent the magnitude of the contact forces with blue corresponding to small forces and red representing large forces. Here, the smallest contact force approaches zero, and the largest is 12.7 kN. It shows that, in the elastic stage, contact forces are distributed evenly in the particle as shown in Figure 7a. Figure 7b shows larger contact forces start to concentrate at the contacts between the particle and the upper platen in the crack initiation stage. At the stress peak, the dense large contact forces appear at the contacts between the particle and the top platen at the strain $\epsilon = 0.029$, as shown in Figure 7c. At $\epsilon = 0.043$ in the softening stage

as shown in Figure 7d, even larger contact forces form perpendicular to the direction of loading, which indicates the future tensile failure of the particle. Figures 7e and 7f show that the contact forces become weakened until the particle loses its bearing capability in the final splitting stage.

Conclusions

The DEM is used as a tool to shed light on the breakage of individual ballast particles loaded between two platens. The irregular shape of the ballast particle is taken into account, and

parallel bonds are adopted in order to prevent the relative rolling between sub-spheres. The simulated tensile strength agrees well with the physical experimental data from the published literature. The value is smaller compared with that obtained by published DEM results with a more spherical description of ballast particle.

The stress-strain relationship of a typical ballast particle is analysed, and four stages, linear elastic, crack initiation, softening and final splitting are identified. The corresponding failure modes at different failure stages are depicted. The internal breakage mechanism is further examined from the microscopic point of view. The bond breakage numbers are counted and contact force distributions are analysed. The changes of the microscopic variables are consistent with the exhibited macro behaviours of railway ballast. In the linear elastic stage, the particle deforms elastically with no bond breakage and an even distribution of contact force. The crack initiates with few bond breakages and a concentration of contact force at the contact between the particle and upper flatten in the crack initiation stage. During softening, stress drops with more bond breakages and the formation of larger contact forces perpendicular to the loading direction. Finally, the particle splits into smaller pieces with a rapid increase of bond breakages and weakening of contact forces in the splitting stage. Future studies will deal with the effect of particle breakage on the track settlement with the developed DEM models through box tests which simulate train loading.

Funding

This work was supported by National Natural Science Foundation of China Key Project- Joint Fund of High Speed Railway Basic Research [Grant No. U1234209], and the National Program on Key Basic Research Project (973 Program) [2010CB731502].

References

- Cheng, Y.P., Bolton, M.D. and Nakata, Y., 2004. Crushing and plastic deformation of soils simulated using DEM. *Geotechnique*, 54 (2), 131–141.
- Cheng, Y.P., Nakata, Y. and Bolton, M.D., 2003. Discrete element simulation of crushable soil. *Geotechnique*, 53 (7), 633–641.
- Cho, G.C., Dodds, J. and Santamarina J.C., 2006. Particle shape effects on packing density, stiffness, and strength: natural and crushed sands. *Journal of Geotechnical and Geoenvironmental Engineering*, 132 (5), 591–602.
- Cho, N., Martin, C.D. and Sego, D.C., 2007. A clumped particle model for rock. *International Journal of Rock Mechanics & Mining Sciences*, 44, 997–1010.
- Cil, M.B. and Alshibli, K.A., 2012. 3D assessment of fracture of sand particles using discrete element method. *Geotechnique Letters*, 2, 161–166.
- Darvell, B.W., 1990. Uniaxial compression tests and the validity of indirect tensile strength. *Journal of Materials Science*, 25, 757–780.
- Davidge, R.W., 1979. *Mechanical behaviour of ceramics*. London: Cambridge University Press.
- Ergenzinger, C., Seifried, R. and Eberhard, P., 2012. A discrete element approach to model breakable railway ballast. *Journal of Computational and Nonlinear Dynamics*, 7, 041010-1–04010-8.
- Esveld, C., 2001. *Modern railway track*, Zaltbommel: MRT-Productions.
- Ferrellec, J.F. and McDowell, G.R., 2008. A simple method to create complex particle shapes for DEM. *Geomechanics and Geoengineering: An International Journal*, 3 (3), 211–216.
- Ferrellec, J.F. and McDowell, G.R., 2010. A method to model realistic particle shape and inertia in DEM. *Granular Matter*, 12 (5), 459–467.
- Hanley, K.J., O’Sullivan, C., Oliveira, J.C., Cronin, K. and Byrne, E. P., 2011. Application of Taguchi methods to DEM calibration of bonded agglomerates. *Powder Technology*, 210, 230–240.
- Hess, W. and Schonert, K., 1981. Brittle-plastic transition in small particles. In: *Powtech Conference on Particle Technology*, March 5–7, Birmingham, EFCE event No. 241. Rugby: Institution of Chemical Engineers, D2/I/1–D2/I/9.
- Housain, Z., Indraratna, B., Darve, F. and Thakur, P., 2007. DEM analysis of angular ballast breakage under cyclic loading. *Geomechanics and Geoengineering: International Journal*, 2 (3), 175–182.
- Indraratna, B., Nimbalkar, S. and Christie, D., 2009. The performance of rail track incorporating the effects of ballast breakage, confining pressure and geosynthetic reinforcement. In: *8th International Conference on the Bearing Capacity of Roads, Railways, and Airfields*, June 29 - July 2. London: Taylor and Francis Group, 5–24.
- Indraratna, B., Thakur, P.K. and Vinod, J.S., 2010. Experimental and numerical study of railway ballast behaviour under cyclic loading. *International Journal of Geomechanics, ASCE*, 10 (4), 136–144.
- Itasca, 1999. *Particle flow code in 3 dimensions*. Minneapolis: Itasca Consulting Group, Inc.
- Jaeger, J.C., 1967. Failure of rocks under tensile conditions. *International Journal of Rock Mechanics and Mining Sciences*, 4, 219–227.
- Ji, S., 2013. Probability analysis of contact forces in quasi-solid-liquid phase transition of granular shear flow. *Science China - Physics, Mechanics & Astronomy*, 56 (2), 395–403.
- Ji, S. and Di, S., 2013. Discrete element modeling of acoustic emission in rock fracture. *Theoretical & Applied Mechanics Letters*, 3 (2), 021009.
- Ji, S., Hanes, D.M. and Shen, H.H., 2009. Comparisons of physical experiment and discrete element simulations of sheared granular materials in an annular shear cell. *Mechanics of Materials*, 41, 764–776.
- Kun, F. and Herrmann, H.J., 1996. A study of fragmentation processes using a discrete element method. *Computer Methods in Applied Mechanics and Engineering*, 138, 3–18.
- Lim, W.L. and McDowell, G.R., 2005. Discrete element modeling of railway ballast. *Granular Matter*, 7, 19–29.
- Lim, W.L. and McDowell, G.R., 2007. The importance of coordination number in using agglomerates to simulate crushable particles in the discrete element method. *Geotechnique*, 57 (8), 701–705.
- Lim, W.L., McDowell, G.R. and Collop, A.C., 2004. The application of Weibull statistics to the strength of railway ballast. *Granular Matter*, 6, 229–237.
- Lobo-Guerrero, S. and Vallejo, L.E., 2006. Discrete element method analysis of railtrack ballast degradation during cyclic loading. *Granular Matter*, 8, 195–204.

- McDowell, G.R. and Amon, A., 2000. The application of Weibull statistics to the fracture of soil particles. *Soils and Foundations*, 40 (5), 133–142.
- McDowell, G.R. and Bolton, M.D., 1998. On the micromechanics of crushable aggregates. *Geotechnique*, 48 (5), 667–679.
- Peters, B. and Dziugys, A., 2002. Numerical simulation of the motion of granular material using object-oriented techniques. *Computer Methods in Applied Mechanics and Engineering*, 191, 1983–2007.
- Potyondy, D.O. and Cundall, P.A., 2004. A bonded-particle model for rock. *International Journal of Rock Mechanics & Mining Sciences*, 41, 1329–1364.
- Russell, A.R. and Muir Wood, D., 2009. Point load tests and strength measurements for brittle spheres. *International Journal of Rock Mechanics and Mining Sciences*, 46, 272–280.
- Selig, E.T. and Waters, J.M., 1994. *Track geotechnology and sub-structure management*. London: Thomas Telford.
- Tang, C.A., Xu, X.H., Kou, S.Q., Lindqvist, P.A. and Liu, H.Y., 2001. Numerical investigation of particle breakage as applied to mechanical crushing-Part I: Single-particle breakage. *International Journal of Rock Mechanics & Mining Sciences*, 38, 1147–1162.
- Yan, Y. and Ji, S., 2010. Discrete element modeling of direct shear tests for a granular material. *International Journal for Numerical and Analytical Methods in Geomechanics*, 34 (9), 978–990.